ResearchGate

See discussions, stats, and author profiles for this publication at: https://www.researchgate.net/publication/259697646

Virtual screening of mandelate racemase mutants with enhanced activity based on binding energy in the transition state

ARTICLE · FEBRUARY 2014

DOI: 10.1016/j.enzmictec.2013.10.008 · Source: PubMed

CITATIONS
5

READS
88

9 AUTHORS, INCLUDING:

Jiali Gu
Zhejiang University
16 PUBLICATIONS **78** CITATIONS
SEE PROFILE

Wenping Xie
dyg-hec
13 PUBLICATIONS **50** CITATIONS
SEE PROFILE

Wenqiang Lu
Zhejiang University
9 PUBLICATIONS **35** CITATIONS
SEE PROFILE

HongWei Yu
Zhejiang University
60 PUBLICATIONS **465** CITATIONS
SEE PROFILE

All in-text references underlined in blue are linked to publications on ResearchGate, letting you access and read them immediately.

Available from: HongWei Yu
Retrieved on: 27 January 2016

Enzyme and Microbial Technology 55 (2014) 121–127

Contents lists available at ScienceDirect

Enzyme and Microbial Technology

journal homepage: www.elsevier.com/locate/emt

Virtual screening of mandelate racemase mutants with enhanced activity based on binding energy in the transition state

Jiali Gu, Min Liu, Fei Guo, Wenping Xie, Wenqiang Lu, Lidan Ye, Zhirong Chen, Shenfeng Yuan, Hongwei Yu *

Department of Chemical and Biological Engineering, Zhejiang University, Hangzhou 310027, PR China

ARTICLE INFO

Article history:
Received 7 June 2013
Received in revised form 22 October 2013
Accepted 23 October 2013

Keywords:
Virtual screening
Mandelate racemase
Binding energy
Transition state
Molecular dynamics simulation

ABSTRACT

Mandelate racemase (MR) is a promising candidate for the dynamic kinetic resolution of racemates. However, the poor activity of MR towards most of its non-natural substrates limits its widespread application. In this work, a virtual screening method based on the binding energy in the transition state was established to assist in the screening of MR mutants with enhanced catalytic efficiency. Using *R*-3-chloromandelic acid as a model substrate, a total of 53 mutants were constructed based on rational design in the two rounds of screening. The number of mutants for experimental validation was brought down to 17 by the virtual screening method, among which 14 variants turned out to possess improved catalytic efficiency. The variant V26I/Y54V showed 5.2-fold higher catalytic efficiency (k_{cat}/K_m) towards *R*-3-chloromandelic acid than that observed for the wild-type enzyme. Using this strategy, mutants were successfully obtained for two other substrates, *R*-mandelamide and *R*-2-naphthylglycolate (V26I and V29L, respectively), both with a 2-fold improvement in catalytic efficiency. These results demonstrated that this method could effectively predict the trend of mutational effects on catalysis. Analysis from the energetic and structural assays indicated that the enhanced interactions between the active sites and the substrate in the transition state led to improved catalytic efficiency. It was concluded that this virtual screening method based on the binding energy in the transition state was beneficial in enzyme rational redesign and helped to better understand the catalytic properties of the enzyme.

© 2013 Elsevier Inc. All rights reserved.

1. Introduction

Due to its remarkable stability and broad substrate spectrum, mandelate racemase (MR) is an attractive catalyst for the racemization of α-hydroxy carboxylic acids. However, except for the electron-withdrawing substituent in the *p*-position of the aryl moiety, MR shows poor activity against the non-natural substrates [1]. Hence, it is of great scientific interest to reconstruct the enzyme for enhanced catalytic performance.

Currently, two major reconstruction strategies are applied in enzymatic engineering: directed evolution and rational design. High-throughput screening methods are limited for directed evolution of racemase, while rational design is a suitable choice since the crystal structure of mandelate racemase is available and the catalytic mechanism is well studied [2,3]. However, the efficiency of rational design could not meet the requirement of enzyme engineering [4,5]. Therefore, it is necessary to improve its efficiency.

Virtual screening is a promising approach to enhance the efficiency of rational design, which is facilitated via a quick search of the large enzyme library based on computational simulation to identify potential candidates for further experimental validation. However, there are few reports about its application in enzyme redesign, probably due to the lack of generally accepted screening standards. Recently, Zheng et al. employed virtual screening to facilitate the screening of cocaine hydrolase mutants with improved activity, using the interaction energy and energy barrier as the screening criteria [6]. On one hand, they did not consider the solvation effect and intramolecular interactions during the calculation of interaction energy, which might lead to reduced accuracy. On the other hand, the energy barrier calculation performed by the sophisticated and hybrid quantum mechanical/molecular mechanical (QM/MM) simulation was time-consuming and CPU-demanding. Therefore, it is necessary to develop an alternative route with reasonable accuracy and acceptable time cost.

Binding energy is of fundamental importance for enzyme catalysis [7]. Enzymes use substrate-binding energy not only to promote

* Corresponding author at: Institute of Bioengineering, Department of Chemical and Biological Engineering, Zhejiang University, Hangzhou 310027, PR China. Tel.: +86 571 8795 1873.
E-mail address: yuhongwei@zju.edu.cn (H. Yu).

0141-0229/$ – see front matter © 2013 Elsevier Inc. All rights reserved.
http://dx.doi.org/10.1016/j.enzmictec.2013.10.008

the ground-state association, but also to stabilize the reaction transition state, reducing the energy barrier of the catalytic process [8]. The virtual dissociation constant of the enzyme-substrate complex in the transition state (K_{tx}) is defined by the Eq. (1)

$$K_{tx} = \frac{k_{non}}{k_{cat}/K_m} \quad (1)$$

where k_{non} is the rate constant of the non-enzymatic reaction, k_{cat} is the turnover number, K_m is the Michaelis constant [9]. The binding energy of the enzyme-substrate complex in the transition state is calculated as follows:

$$\Delta G = -RT \ln\left(\frac{1}{K_{tx}}\right) = -RT \ln\left(\frac{k_{cat}/K_m}{k_{non}}\right)$$

$$= RT \ln(k_{non}) - RT \ln\left(\frac{k_{cat}}{K_m}\right) \quad (2)$$

For enzymes that catalyze the same reaction, the k_{non} value is fixed, the catalytic efficiency of these enzymes could thus be compared based on their difference in the binding energy ($\Delta\Delta G$):

$$\Delta\Delta G = \Delta G_2 - \Delta G_1 = RT \ln\left(\frac{k_{cat}}{K_m}\right)_1 - RT \ln\left(\frac{k_{cat}}{K_m}\right)_2$$

$$= RT \ln\left(\frac{(k_{cat}/K_m)_2}{(k_{cat}/K_m)_1}\right) \quad (3)$$

Great effort has been made to develop computational methods that allow reliable estimation of the binding energy for a given catalytic process [10–12]. Among them, molecular mechanics/Poisson–Boltzmann surface area (MM/PBSA) is widely used to provide relatively accurate binding energy values at moderate computational cost [13–15]. In addition, the MM/PBSA approach allows for the analysis of individual energy contributions by means of free energy decomposition, which gives additional energetic insights to the system of interest. Therefore, calculation of binding energy based on MM/PBSA could be suitable for the virtual screening.

Herein, we aimed to develop a virtual screening method based on the binding energy of the enzyme-substrate complex in the transition state to facilitate the screening of positive MR mutants towards non-natural substrates. Using *R*-3-chloromandelic acid as a model substrate, the binding energies of variants from the mutant library were calculated and the potential candidates were selected for further experimental investigation. The mechanisms behind the improved catalytic efficiency were studied from the perspective of energy and structure. Furthermore, the screening method was applied to screen positive variants towards two other non-natural substrates (*R*-2-naphthylglycolate and *R*-mandelamide).

2. Materials and methods

R-3-chloromandelic acid and all other reagents, unless mentioned otherwise, were purchased from Sigma–Aldrich Chemical Company. Recombinant mandelate racemase from *Pseudomonas putida* containing the MR open reading frame (ORF) and N-terminal hexahistidine tag was overproduced and purified from *Escherichia coli* strain BL21 cells transformed with a pET-30a plasmid (Novagen, Madison, WI). The enzyme was purified by metal ion affinity chromatography as described in the Novagen protocols. The purity of the enzyme was confirmed by SDS-PAGE (Fig. S1).

2.1. Site-directed mutagenesis

The pET-30a plasmid containing the recombinant MR gene was used as a template for polymerase chain reaction (PCR)-based site directed mutagenesis. Site directed mutagenesis was performed by using the QuikChange™ method (Stratagene, La Jolla, CA). The two synthetic primers used to construct the mutants were listed in Table S1 in the supplementary material. The genes of the mutants were sequenced to verify that no other alterations in the nucleotide sequence were introduced. The mutants were purified using the same procedure as described for the wild-type enzyme.

2.2. Enzyme assay

MR activity was assayed at 25 °C in HEPES-buffer (100 mM, pH 7.5, 3.3 mM $MgCl_2{\cdot}2H_2O$) based on the online measurement of the change of the optical rotation versus time using a Rudolph Research Autopol IV Automatic Polarimeter. Spontaneous racemization under the reaction conditions was checked for all the substrates in the absence of enzyme and was proven to be <3% within 72 h. For all assays, the substrate solutions were incubated at 25 °C prior to the reaction, and the concentrations of substrates ranged from 0.15 to 10 mM. Reactions were initiated by addition of the enzyme to give a final enzyme concentration of 1–100 ng ml^{-1}.

2.3. Data analysis

The values of V_{max} and K_m were determined from plots of the initial velocity (V_i) versus the substrate concentration [*S*]) by fitting the data to Eq. (4) using nonlinear regression analysis. All kinetic parameters were determined in triplicate. The protein concentration was measured by absorption spectroscopy in a UV-2800 UV/Vis Spectrophotometer using the BSA kit (Bio-Rad) and k_{cat} values were obtained by dividing the V_{max} values by the total enzyme concentration ($[E]_t$).

$$V_i = \frac{V_{max}[S]}{K_m + [S]} \quad (4)$$

2.4. Molecular dynamic (MD) simulation

The starting geometry coordinates for the calculation were taken from the 2.2 Å resolution X-ray crystal structure of the MR with the analogue of putative *aci*-carboxylate intermediate, benzohydroxamate (PDB ID: 3UXK) [16]. The *aci*-carboxylate intermediate, taken as the transition state, was located in the active site to match the maximum number of atoms with benzohydroxamate in the X-ray structure. Partial charges and force field parameters of the substrates were generated automatically by the antechamber programme using the general AMBER force field (GAFF) [17,18]. The non-polar hydrogen atoms were added to the enzyme by AMBER 11 simulation package using the ff10 force field. The protonation state of all the residues was set according to pH 7.0, except Glu317, which was protonated to reproduce the hydrogen bond with the carboxyl oxygen atom of substrate. Both the ε-N and δ-N of residue His 297 were protonated in the transition state. Residues 86–101 from the related subunit, which are located around the active site, were added to the protein model [19]. Counterions of Na^+ were added to neutralize the system and the whole system was immersed in a rectangle box of TIP3P water molecules [20], extended 10 Å from the dissolved atoms in all three dimensions. Each MD simulation included minimization, heating, density equilibration at constant temperature, equilibration under constant pressure (NPT) and production run in the NPT ensemble according to our previous work [21].

2.5. MM/PBSA analysis

The calculation and decomposition of binding energy between the ligand and the enzyme was evaluated using the MM/PBSA method as implemented in AMBER 11 with a thermodynamic cycle that combined the molecular mechanical energies with the continuum solvent approach. As many as 100 snapshots were taken after the MD trajectory of enzyme-substrate complex reached a plateau. The binding energy ΔG_{bind} between a ligand (L) and a receptor (R) required for forming a complex (C) was calculated as follows:

$$\Delta G_{bind} = \Delta H - T\Delta S \approx \Delta E_{MM} + \Delta G_{sol} - T\Delta S$$

$$\Delta E_{MM} = \Delta E_{internal} + \Delta E_{electrostatic} + \Delta E_{vdw}$$

$$\Delta G_{sol} = \Delta G_{PB} + \Delta G_{np}$$

where ΔE_{MM}, ΔG_{sol}, $T\Delta S$, stand for the changes of the gas phase MM energy, the solvation free energy, and the conformational entropy, respectively. ΔE_{MM} is the sum of $\Delta E_{internal}$ (bonds, angles and dihedrals energy), $\Delta E_{electrostatic}$ (electrostatic energy), and ΔE_{vdw} (van der Waals). G_{sol}, which accounts for the solvation energy, is divided into the electrostatic solvation energy (ΔG_{PB}) and the non-polar solvation energy (ΔG_{np}). The entropic contributions were excluded due to the little contribution of entropy to the stabilization of the transition state [22], the cancelling out of entropic contribution in the binding energy difference between the wild type and mutants [23–25], and the time-consuming nature of entropy determination [26]. The dielectric constants inside and outside the molecule were 1.0 and 80.0, respectively. "The single-trajectory method" [27,28] was used where the internal energy term ($\Delta E_{internal}$) was zero.

2.6. Statistical analysis

F-test and Student's *t* test were performed to test if the difference between the wild type and the mutants in the binding energy was significant. Based on the mean

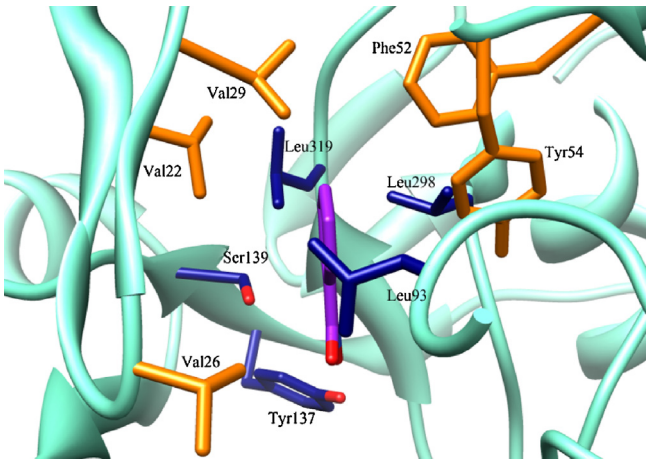

Fig. 1. Residues involved in the mutant library. The *aci*-carboxylate intermediate, benzohydroxamate is illustrated in purple; residues from hydrophobic pocket are shown in orange, while the other residues are shown in blue. (For interpretation of the references to color in this figure legend, the reader is referred to the web version of the article.)

values (μ_1 and μ_2) and the standard deviations (S_1^2 and S_2^2) of the binding energy for the wild type and the mutants, the *F*-test is calculated as:

$$F = \frac{\max(S_1^2, S_2^2)}{\min(S_1^2, S_2^2)}$$

and the *t*-statistic is calculated as:

$$t = \frac{\mu_1 - \mu_2}{S_w \times \sqrt{(1/n_1) + (1/n_2)}}$$

$$S_w = \sqrt{\frac{(n_1 - 1) \times S_1^2 + (n_2 - 1) \times S_2^2}{(n_1 + n_2 - 2)}}$$

where n_1 and n_2 are the numbers of observations (here, both n_1 and n_2 were 100).

The variances and the mean values of the binding energy for the wild type and mutants were considered significantly different at 95% confidence level if the absolute values of the *F*-statistic and *t*-statistic were above 1.417 and 1.658, respectively. Only the mutants with significantly lower binding energy, compared to the wild type, were subjected to experimental validation.

3. Results

3.1. Construction of the first-round mutant library

The mutant library in virtual screening was generated based on the structure-function relationship. It was reported that the majority of mutations beneficially affecting enzyme enantioselectivity, substrate specificity or new catalytic activity were related to the residues that participated in substrate binding or catalysis [29–31]. Therefore, the mutant library in the present work was constructed by generating mutations in the residues from the 20s/50s loops related to substrate specificity and from the active sites (Fig. 1). The residues in the 20s/50s loops interact with the phenyl group of the substrate mainly through van der Waals (VDW) interactions [19,32]. Residues Val22 and Val29 are located at the beginning and the end of the 20s loop, and Val 26 is located near the tip of the flap. Residues Phe52 and Tyr54 from the 50s loop are located directly towards the substrate. As shown in Fig. 1, several residues in the active cavity which might also be involved in the process of catalysis are considered, including residue Leu93 (from an adjacent subunit), Tyr137 and Ser139 (interact with the carboxyl group of the substrate), as well as Leu298 and Leu319 (interact with the phenyl group of the substrate through hydrophobic interaction). These ten residues were mutated based on their properties and proposed functions during catalysis. Finally, a library containing 40 mutants was generated (Table S2).

3.2. Virtual screening of potential candidates and experimental test

The molecular dynamics (MD) simulations were carried out for the wild type and mutants from the library with *R*-3-chloromandelic acid in the transition state and the corresponding binding energies were calculated by the MM/PBSA approach (Table S2). The binding energy for the wild type with *R*-3-chloromandelate complex was about −24 kcal/mol, higher than the binding energy observed for the natural substrate mandelate (−26 kcal/mol) [33]. To select out variants with significantly decreased binding energy, Student's *t* test was carried out. As shown in Table S2 and Table S3, 25 mutants showed significantly increased binding energy, 1 showed no significant change in binding energy, while only 14 achieved significantly decreased binding energy, which were thus chosen as potential candidates for verification. These 14 mutants were then directly used for determination of kinetic parameters without removing the hexahistidine tag, since it was reported that the presence or absence of the His-tag hardly influence the kinetic parameters for the recombinant enzyme [34]. The results demonstrated that 12 variants exhibited enhanced catalytic efficiency, ranging from 1.2-fold to 3.7-fold improvement (Table 1). With the exception of L319F, all other 11 positive mutants were from the 20s/50s loops. It was found that replacement of Tyr54 with hydrophobic residues (Ala, Ile, Leu, Val, Phe) could enhance the catalytic efficiency. All the positive mutants displayed substrate binding affinity (K_m) similar to that of the wild type, except Y54I. While all the positive mutants exhibited higher k_{cat} values, except mutant V29L. Mutant V26L exhibited the highest improvement in the catalytic efficiency (3.7 fold), which was mainly due to the increased k_{cat} value (3.7 fold).

3.3. Second round of screening and experimental validation

Based on the results from the first round of screening, 6 mutants (V22L, V26I, V26L, Y54V, Y54I, L319F) with catalytic efficiency improvements of at least 2-fold were selected to construct the mutant library in the second round of screening. A library containing 13 double-point mutants was generated and the corresponding binding energy in the transition state was estimated (Table S2). Only 3 mutants (V26I/Y54I, V26I/Y54V, V26L/Y54I) were selected for further verification since they displayed significantly decreased binding energy (Table S2, Table S3). And it turned out that mutants V26I/Y54I and V26I/Y54V exhibited improved catalytic efficiency. For both mutants, the k_{cat} values were dramatically increased, while the substrate binding affinity (K_m) for V26I/Y54V was lower than that observed for the wild type. The mutant V26I/Y54V showed the highest improvement in the catalytic efficiency (5.2 fold), in accordance with the simulation results that it had the lowest binding energy (−29.14 kcal/mol).

3.4. Binding energy decomposition and structural analysis

To explain the improvement in the catalytic efficiency, the binding energy of the wild type and 14 positive mutants was decomposed and the binding contribution from each residue was estimated. On one hand, the energy contribution from the active sites (Ser139, Lys164, Lys166, Asn197, His 297, Glu317) was much higher than those from the 20s loop and 50s loop, accounting for a major proportion of the total binding energy in the transition state (Table S4). On the other hand, the fluctuation of total energy was mainly due to the changes in energy contribution of residues located within or proximal to the active sites rather than those of

Table 1
Kinetic parameters of the wild type and mutants towards *R*-3-chloromandelic acid, *R*-mandelamide and *R*-2-naphthylglycolate.

	K_m (mM)	k_{cat} (s^{-1})	k_{cat}/K_m ($M^{-1}\ s^{-1}$)
R-3-Chloromandelic acid			
WT	1.89 ± 0.05	$(4.69 \pm 0.12) \times 10^2$	$(2.49 \pm 0.11) \times 10^5$
V22L	2.40 ± 0.18	$(1.22 \pm 0.05) \times 10^3$	$(5.09 \pm 0.21) \times 10^5$
V22I	2.12 ± 0.05	$(6.37 \pm 0.11) \times 10^2$	$(3.00 \pm 0.11) \times 10^5$
V26L	1.87 ± 0.08	$(1.71 \pm 0.07) \times 10^3$	$(9.16 \pm 0.22) \times 10^5$
V26I	2.46 ± 0.10	$(2.02 \pm 0.05) \times 10^3$	$(8.21 \pm 0.24) \times 10^5$
V26S	1.90 ± 0.07	$(5.59 \pm 0.14) \times 10^2$	$(2.94 \pm 0.12) \times 10^5$
V29L	1.27 ± 0.06	$(3.88 \pm 0.08) \times 10^2$	$(3.05 \pm 0.15) \times 10^5$
Y54I	3.02 ± 0.70	$(1.52 \pm 0.05) \times 10^3$	$(5.02 \pm 0.20) \times 10^5$
Y54V	2.17 ± 0.20	$(1.16 \pm 0.05) \times 10^3$	$(5.33 \pm 0.18) \times 10^5$
Y54A	2.22 ± 0.10	$(9.53 \pm 0.15) \times 10^2$	$(4.29 \pm 0.25) \times 10^5$
Y54L	1.62 ± 0.08	$(5.65 \pm 0.09) \times 10^2$	$(3.49 \pm 0.20) \times 10^5$
Y54F	1.95 ± 0.06	$(5.07 \pm 0.11) \times 10^2$	$(2.59 \pm 0.12) \times 10^5$
L319F	1.72 ± 0.08	$(9.13 \pm 0.19) \times 10^2$	$(5.31 \pm 0.20) \times 10^5$
V26I/Y54V	3.92 ± 0.32	$(5.10 \pm 0.12) \times 10^3$	$(1.30 \pm 0.10) \times 10^6$
V26I/Y54I	1.99 ± 0.09	$(1.03 \pm 0.08) \times 10^3$	$(5.15 \pm 0.25) \times 10^5$
R-Mandelamide			
WT	1.13 ± 0.05	11.03 ± 0.50	$(9.79 \pm 0.22) \times 10^3$
V26I	1.24 ± 0.10	21.17 ± 0.15	$(1.71 \pm 0.14) \times 10^4$
R-2-Naphthylglycolate			
WT[a]	1.20 ± 0.10	46.00 ± 1.00	$(3.80 \pm 0.20) \times 10^4$
WT[a,b]	3.50 ± 0.20	70.00 ± 3.00	$(2.01 \pm 0.03) \times 10^4$
V22I[a,b]	4.20 ± 0.20	147.00 ± 2.00	$(3.40 \pm 0.10) \times 10^4$
V29L[a]	1.60 ± 0.10	137.00 ± 6.00	$(8.50 \pm 0.20) \times 10^4$

WT: the wild type enzyme.
[a] Kinetic parameters determined by the L. Bearne group.
[b] Kinetic parameters determined using 20 mM Mg^{2+}.

residues in the 20s/50s loops (Fig. S2). As shown in Fig. 2, there were no obvious contribution differences from the residues in the 20s/50s loops between the wild type and the variants. However, binding contributions from the residues in the active site for the positive variants were higher than those for the wild type. For the variant V26I/Y54V, the contributions from catalytic residues Lys164, Lys166 and His297 were 4.5, 1.1 and 3.5 kcal/mol higher, respectively. Further structural investigation demonstrated that compared with the wild type, for the positive mutants, the hydrogen bond (HB) angle between residues Ser139, Lys164, Glu317 and the substrate was usually larger while the HB distance was relatively shorter, indicating a tighter hydrogen bond interaction (Fig. 3, Fig. 4 and Table S5). For mutant V26I/Y54V, the HB angle (a3) between Lys164 and the substrate was 10 degree larger, while the HB distance (d3) was 0.08 Å shorter. The same phenomena were observed for two other hydrogen bonds. Thus, the alteration of the interaction between the active cavity and the substrate was the key factor leading to an enhancement in the catalytic efficiency.

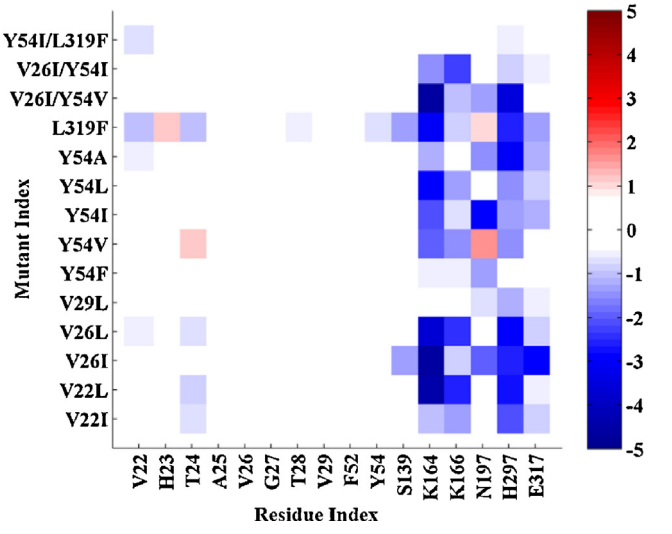

Fig. 2. Binding contribution differences from the residues in the 20s/50s loops and the active cavity between the wild type and positive mutants. The contribution difference for each residue was calculated by the contribution value for the positive mutants minus the corresponding value for the wild type. The binding energy contribution difference ranges from blue (most negative) to red (most positive). (For interpretation of the references to color in this figure legend, the reader is referred to the web version of the article.)

3.5. Application of the virtual screening model for other non-natural substrates

To further evaluate the efficiency of the present virtual screening protocol, two other non-natural substrates (*R*-2-naphthylglycolate and *R*-mandelamide) were investigated.

R-2-Naphthylglycolate (*R*-2-NG), a bulky substrate, was employed to probe the effect of steric bulk of the 20s loop on the MR function by L. Bearne et al. [32]. In our study, a mutant library

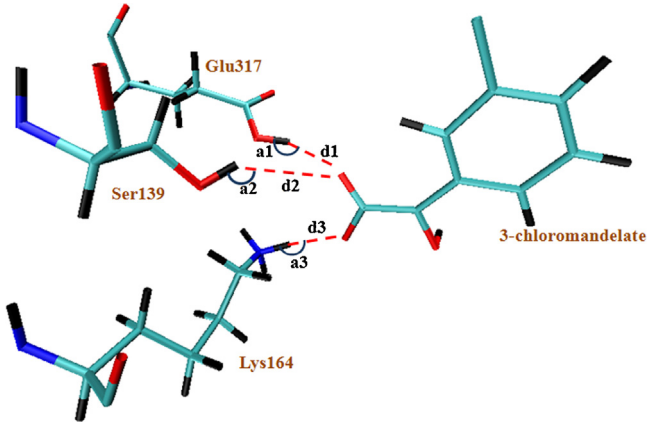

Fig. 3. Hydrogen bonds formed between the residues Ser139, Lys164, Glu317 and substrate.

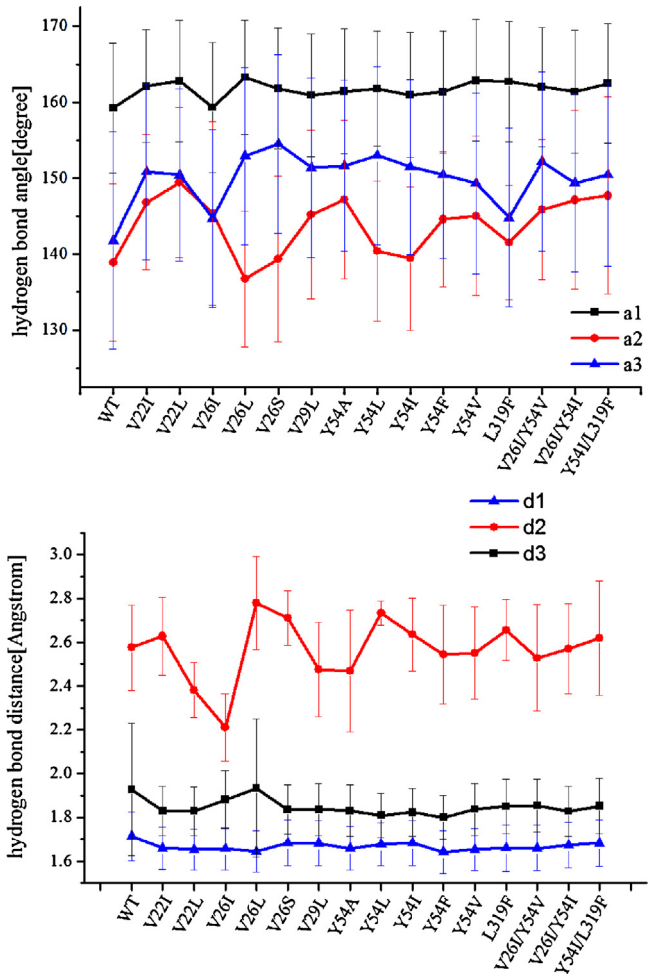

Fig. 4. Angles and distances of hydrogen bond between Ser139, Lys164, Glu317 and substrate for the wild type and positive mutants. WT: the wild type.

including 11 mutants was generated based on their report. The MD simulations of mutants with *R*-2-NG in the transition state were carried out and the virtual screening based on the binding energy was followed (Table S6). Two variants (V22I, V29L) were selected out as the potential candidates, which had a good agreement with the experimental results that the catalytic efficiencies of the mutants V22I and V29L were 1.7-fold and 2.2-fold higher than that of the wild type, respectively.

Mandelamide is a typical non-natural substrate where the carboxylate moiety is substituted by carboxamide. It was racemized at a rate 5-fold lower than mandelate [1]. Based on the results from *R*-3-chloromandelic acid, a mutant library was constructed with 22 mutants from the 20s/50s loops. Among the 22 mutants, only V26I and V29A showed significantly lower binding energies than that of the wild type (Table S7). The subsequent investigation demonstrated that the mutant V26I displayed a 2-fold increase in the catalytic efficiency, mainly resulted from the increased k_{cat} value (Table 1)

Using the virtual screening method, we successfully acquired positive variants for *R*-2-naphthylglycolate and *R*-mandelamide, suggesting that our approach could be applied to screen MR mutants with improved catalytic activity for other substrates.

4. Discussion

MR from *pseudomonas putida* ATCC 12633 catalyzes the Mg^{2+}-dependent 1,1-proton transfer which interconverts the (*R*) and (*S*)-enantiomers of mandelic acid. Its catalytic mechanism and enzymatic properties have been studied in detail [21,35–37]. However, the redesign of MR for enhanced performance or new catalytic properties has never been reported, which might be due to the lack of a proper high-throughput screening method.

In the present work, a virtual screening method based on the binding energy in the transition state was developed to assist rational design to obtain positive MR mutants towards non-natural substrates. In the case of *R*-3-chloromandelate, 17 potential mutants from a total of 53 designed variants were selected out, and among them 14 mutants exhibited improved catalytic efficiency. The high efficiency of this approach was also observed in the cases of two other substrates (*R*-2-naphthylglycolate and *R*-mandelamide). Therefore, the virtual screening method could dramatically reduce the number of variants for experimental verification and improve the efficiency of rational design. The reason for the high efficiency probably lies in the following aspects. Firstly, as shown in Eq.2, the binding energy in the transition state is directly related to the catalytic efficiency in its exponential form, which indicates that it is able to predict the mutational effect on the catalysis based on the binding energy. Secondly, Amber force fields, which are the most popular biomolecular force field, guaranteed reliable conformational ensembles in the simulation of enzymatic processes [38,39]. Thirdly, an adequate conformational ensemble (100 snapshots from the MD trajectories) was fundamental for the accurate energy estimation in this study [40]. Finally, the high accuracy of the binding energy calculated by MM/PBSA also ensured the high efficiency of the screening method, which combines explicit solvent MD simulations with the Poisson–Boltzmann calculations of the solvation energy and the solvent accessible surface area-based non-polar solvation free energy calculations [28,41,42].

Moreover, another advantage of the present strategy was the decreased computational cost. Typically, the screening process of 14 mutants (20 runs for each mutant) using EVB took 24 h and needed to be performed on 200 nodes due to the extensive sampling required for achieving physically meaningful convergent free energy [43]. In contrast, the whole molecular dynamics simulation and binding energy calculation process for mandelate racemase (396 amino acids) using the molecular mechanical method facilitated by AMBER software in this work could be completed within about 50 min per node under the Inspur Tiansuo cluster (152× Intel Xeon CPU, 608 cores), suggesting the feasibility of our strategy for the identification of a large number of mutants.

All positive mutants except L319F were from the 20s loop and 50s loop, which accommodate the phenyl group of *R*-enantiomer and *S*-enantiomer, respectively. Improving the enzymatic activity or enantioselectivity by engineering the substrate binding and access channel was already reported in models such as lipases from *Burkholderia cepacia* [44] and *Candida antarctica* [45]. In the present study, it was found that alteration of steric bulk of residues in the 20s loop had a minimal effect on the substrate binding affinity (K_m), in accordance with the fact that the 20s loop was flexible, the conformational rearrangement of the loop would compensate for the different steric hindrance [32]. Varying the size of residues in the 20s loop and 50s loop had an obvious impact on the k_{cat} value, suggesting that the catalytic efficiency was altered by the interactions between the engineered loops and the substrate. However, the following analysis from the energetic and structural perspectives demonstrated that the increased interactions (the electrostatic interaction and the hydrogen bond interaction) between the residues in the active cavity and the substrate rather than those from the 20s/50s loops, were the main reason for the improved catalytic efficiency. This was reasonable since the residues in the active cavity of MR interacted with the substrate mainly via electrostatic interactions and hydrogen bond interactions [21,36]. A number of reports have confirmed the dominant

role of electrostatic effect in catalysis [46] and the advantages of hydrogen bond interaction in transition state stabilization [47,48]. Therefore, the effect of varying 20s/50s loops on the catalytic efficiency was indirect, and such phenomena were also observed in lipase after mutation of residues located far from the active cavity [49].

5. Conclusion

In the present work, we developed a virtual screening method based on the binding energy in the transition state to assist in the screening of positive MR mutants against non-natural substrates. Positive variants towards *R*-3-chloromandelic acid, *R*-mandelamide and *R*-2-naphthylglycolate were successfully acquired, which demonstrated that this screening approach was efficient and could be further applied in other enzyme redesign experiments/schemes.

Acknowledgements

This work was financially supported by the Natural Science Foundation of China (Grant No., 21176215 and 21176102) and Outstanding Young Scholar of Zhejiang Province (Grant No., R4110092) and the Programme for Zhejiang Leading Team of S&T Innovation (grant No.2011R50007).

Appendix A. Supplementary data

Supplementary data associated with this article can be found, in the online version, at http://dx.doi.org/10.1016/j.enzmictec.2013.10.008.

References

[1] Felfer U, Goriup M, Koegl ME, Wagner U, Larissegger-Schnell B, Faber K, et al. The substrate spectrum of mandelate racemase: minimum structural requirements for substrates and substrate model. Adv Synth Catal 2005;347:951–61.
[2] Neidhart DJ, Powers VM, Kenyon GL, Tsou AY, Ransom SC, Gerlt JA, et al. Preliminary X-ray data on crystals of mandelate racemase. J Biol Chem 1988;263:9268–70.
[3] Powers VM, Koo CW, Kenyon GL, Gerlt JA, Kozarich JW. Mechanism of the reaction catalyzed by mandelate racemase. 1. Chemical and kinetic evidence for a 2-base mechanism. Biochemistry 1991;30:9255–63.
[4] Frushicheva MP, Cao J, Chu ZT, Warshel A. Exploring challenges in rational enzyme design by simulating the catalysis in artificial kemp eliminase. Proc Natl Acad Sci 2010;107:16869–74.
[5] Toscano MD, Woycechowsky KJ, Hilvert D. Minimalist active-site redesign: teaching old enzymes new tricks. Angew Chem Int Ed 2007;46:3212–36.
[6] Zheng F, Yang WC, Ko MC, Liu JJ, Cho H, Gao DQ, et al. Most efficient cocaine hydrolase designed by virtual screening of transition states. J Am Chem Soc 2008;130:12148–55.
[7] Mader MM, Bartlett PA. Binding energy and catalysis: the implications for transition-state analogs and catalytic antibodies. Chem Rev 1997;97:1281–301.
[8] Fersht AR, Leatherbarrow RJ, Wells TNC. Binding energy and catalysis: a lesson from protein engineering of the tyrosyl-tRNA synthetase. Trends Biochem Sci 1986;11:321–5.
[9] Wolfenden R. Transition state analog inhibitors and enzyme catalysis. Annu Rev Biophys Bioeng 1976;5:271–306.
[10] Deng YQ, Roux B. Computations of standard binding free energies with molecular dynamics simulations. J Phys Chem B 2009;113:2234–46.
[11] Minh DDL. Implicit ligand theory: rigorous binding free energies and thermodynamic expectations from molecular docking. J Chem Phys 2012;137.
[12] Brandsdal BO, Osterberg F, Almlof M, Feierberg I, Luzhkov VB, Aqvist J. Free energy calculations and ligand binding. Adv Protein Chem 2003;66:123–58.
[13] Campanera JM, Pouplana R. MMPBSA decomposition of the binding energy throughout a molecular dynamics simulation of amyloid-beta (Aβ10–35) aggregation. Molecules 2010;15:2730–48.
[14] Obiol-Pardo C, Rubio-Martinez. J. Comparative evaluation of MMPBSA and XSCORE to compute binding free energy in XIAP-peptide complexes. J Chem Inf Model 2007;47:134–42.
[15] Hou T, Wang J, Li Y, Wang W. Assessing the performance of the MM/PBSA and MM/GBSA methods. 1. The accuracy of binding free energy calculations based on molecular dynamics simulations. J Chem Inf Model 2010;51:69–82.
[16] Lietzan AD, Nagar M, Pellmann EA, Bourque JR, Bearne SL, St Maurice M. Structure of mandelate racemase with bound intermediate analogues benzohydroxamate and cupferron. Biochemistry 2012;51:1160–70.
[17] Wang J, Wolf RM, Caldwell JW, Kollman PA, Case DA. Development and testing of a general amber force field. J Comput Chem 2004;25:1157–74.
[18] Wang J, Wang W, Kollman PA, Case DA. Automatic atom type and bond type perception in molecular mechanical calculations. J Mol Graph Model 2006;25:247–60.
[19] Siddiqi F, Bourque JR, Jiang HY, Gardner M, St Maurice M, Blouin C, et al. Perturbing the hydrophobic pocket of mandelate racemase to probe phenyl motion during catalysis. Biochemistry 2005;44:9013–21.
[20] Jorgensen WL, Chandrasekhar J, Madura JD, Impey RW, Klein ML. Comparison of simple potential functions for simulating liquid water. J Chem Phys 1983;79:10.
[21] Gu JL, Yu HW. The role of residue S139 of mandelate racemase: synergistic effect of S139 and E317 on transition state stabilization. J Biomol Struct Dyn 2012;30:585–93.
[22] St Maurice M, Bearne SL. Kinetics and thermodynamics of mandelate racemase catalysis. Biochemistry 2002;41:4048–58.
[23] Massova I, Kollman PA. Computational alanine scanning to probe protein–protein interactions: a novel approach to evaluate binding free energies. J Am Chem Soc 1999;121:8133–43.
[24] Wong S, Amaro RE, McCammon. JA. MM-PBSA captures key role of intercalating water molecules at a protein–protein interface. J Chem Theory Comput 2009;5:422–9.
[25] Kar P, Knecht V. Energetic basis for drug resistance of HIV-1 protease mutants against amprenavir. J Comput Aid Mol Des 2012;26:215–32.
[26] Carlsson J, Aqvist J. Calculations of solute and solvent entropies from molecular dynamics simulations. Phys Chem Chem Phys 2006;8:5385–95.
[27] Huo S, Wang J, Cieplak P, Kollman PA, Kuntz ID. Molecular dynamics and free energy analyses of cathepsin D-inhibitor interactions: Insight into structure-based ligand design. J Med Chem 2002;45:1412–9.
[28] Wang J, Morin P, Wang W, Kollman PA. Use of MM-PBSA in reproducing the binding free energies to HIV-1 RT of TIBO derivatives and predicting the binding mode to HIV-1 RT of efavirenz by docking and MM-PBSA. J Am Chem Soc 2001;123:5221–30.
[29] Park S, Morley KL, Horsman GP, Holmquist M, Hult K, Kazlauskas RJ. Focusing mutations into the *P. fluorescens* esterase binding site increases enantioselectivity more effectively than distant mutations. Chem Biol 2005;12:45–54.
[30] Morley KL, Kazlauskas RJ. Improving enzyme properties: when are closer mutations better. Trends Biotechnol 2005;23:231–7.
[31] Godinho LF, Reis CR, Rozeboom HJ, Dekker FJ, Dijkstra BW, Poelarends GJ, et al. Enhancement of the enantioselectivity of carboxylesterase A by structure-based mutagenesis. J Biotechnol 2012;158:36–43.
[32] Bourque JR, Bearne SLF. Mutational analysis of the active site flap (20s loop) of mandelate racemase. Biochemistry 2008;47:566–78.
[33] Bearne SL, Wolfenden R. Mandelate racemase in pieces: effective concentrations of enzyme functional groups in the transition state. Biochemistry 1997;36:1646–56.
[34] Bearne SL, St Maurice M, Vaughan MD. An assay for mandelate racemase using high-performance liquid chromatography. Anal Biochem 1999;269:332–6.
[35] Fee JA, Hegeman GD, Kenyon GL. Mandelate racemase from *Pseudomonas putida*. Subunit composition and absolute divalent metal ion requirement. Biochemistry 1974;13:2528–32.
[36] Neidhart DJ, Howell PL, Petsko GA, Powers VM, Li R, Kenyon GL, et al. Mechanism of the reaction catalyzed by mandelate racemase 2. Crystal structure of mandelate racemase at 2.5-ang. resolution: identification of the active site and possible catalytic residues. Biochemistry 1991;30:9264–73.
[37] Garcia-Viloca M, Gonzalez-Lafont A, Lluch JM. A QM/MM study of the racemization of vinylglycolate catalyzed by mandelate racemase enzyme. J Am Chem Soc 2001;123:709–21.
[38] Case DA, Cheatham TE, Darden T, Gohlke H, Luo R, Merz KM, et al. The Amber biomolecular simulation programs. J Comput Chem 2005;26:1668–88.
[39] Ponder JW, Case DA. Force fields for protein simulations. Adv Protein Chem 2003;66:27.
[40] Homeyer N, Gohlke H. Free energy calculations by the molecular mechanics Poisson–Boltzmann surface area method. Mol Inform 2012;31:114–22.
[41] Huo S, Wang J, Cieplak P, Kollman PA, Kuntz Molecular Dynamics ID. Free energy analyses of cathepsin D-inhibitor interactions: insight into structure-based ligand design. J Med Chem 2002;45:1412–9.
[42] Lee J, Kim J-S, Seok Cooperativity C. Specificity of cys2his2 zinc finger protein–DNA interactions: a molecular dynamics simulation study. J Phys Chem B 2010;114:7662–71.
[43] Frushicheva MP, Cao J, Warshel Challenges A. Advances in validating enzyme design proposals: the case of kemp eliminase catalysis. Biochemistry 2011;50:3849–58.
[44] Lafaquiere V, Barbe S, Puech-Guenot S, Guieysse D, Cortes J, Monsan P, et al. Control of lipase enantioselectivity by engineering the substrate binding site and access channel. ChemBioChem 2009;10:2760–71.
[45] Marton Z, Léonard-Nevers V, Syrén PO, Bauer C, Lamare S, Hult K, et al. Mutations in the stereospecificity pocket and at the entrance of the active site of

Candida antarctica lipase B enhancing enzyme enantioselectivity. J Mol Catal B: Enzym 2010;65:11–7.
[46] Warshel A, Sharma PK, Kato M, Xiang Y, Liu H, Olsson MHM. Electrostatic basis for enzyme catalysis. Chem Rev 2006;106:3210–35.
[47] Hanoian P, Sigala PA, Herschlag D, Hammes-Schiffer. S. Hydrogen bonding in the active site of ketosteroid isomerase: electronic inductive effects and hydrogen bond coupling. Biochemistry 2010;49:10339–48.
[48] Barroso M, Arnaut LG, Formosinho SJ. The role of reaction energy and hydrogen bonding in the reaction path of enzymatic proton transfers. J Phys Org Chem 2009;22:254–63.
[49] Ma J, Wu L, Guo F, Gu J, Tang X, Jiang L, et al. Enhanced enantioselectivity of a carboxyl esterase from *Rhodobacter sphaeroides* by directed evolution. Appl Microbiol Biotechnol 2012:1–10.